Size-dependent magnetic parameters of fcc FePt nanoparticles: applications to magnetic hyperthermia

2010 J. Phys. D: Appl. Phys. 43 145002

(http://iopscience.iop.org/0022-3727/43/14/145002)

J. Phys. D: Appl. Phys. **43** (2010) 145002 (7pp) doi:10.1088/0022-3727/43/14/145002

Size-dependent magnetic parameters of fcc FePt nanoparticles: applications to magnetic hyperthermia

M S Seehra[1,5], V Singh[1], P Dutta[1], S Neeleshwar[2], Y Y Chen[3], C L Chen[3], S W Chou[4] and C C Chen[4]

[1] Department of Physics, West Virginia University, Morgantown, WV 26506-6315, USA
[2] University School of Basic and Applied Sciences, GGS Indraprastha University, Kashmere Gate, Delhi, India
[3] Institute of Physics, Academia Sinica, Taipei, Taiwan, Republic of China
[4] Department of Chemistry, National Taiwan Normal University, Taipei, Taiwan, Republic of China

E-mail: mseehra@wvu.edu

Received 3 December 2009, in final form 18 February 2010
Published 23 March 2010
Online at stacks.iop.org/JPhysD/43/145002

Abstract

For nominal 3 and 9 nm FePt nanoparticles coated with oleylamine/oleic acid and having a face-centred-cubic (fcc) structure, temperature variations (5–300 K) of magnetization M, ac susceptibility χ' and χ'' for the frequency range $f_m = 0.1$–1000 Hz and electron magnetic resonance (EMR) spectra at 9.28 GHz are reported. X-ray diffraction of the samples shows fcc structure with a lattice constant $a = 3.84$ Å and TEM characterization yields log-normal distributions of the particle sizes with average $D = 3.15(0.16)$ nm and $D = 8.70(0.12)$ nm for the 3 nm and 9 nm samples, respectively. M versus T data for the zero-field-cooled and field-cooled modes yield a blocking temperature $T_B = 15$ K (85 K) for the 3 nm (9 nm) samples whereas the hysteresis loops at 5 K yield a coercivity $H_c = 0$ Oe (1.4 kOe). Analysis of the data of T_B at different f_m determined from the peaks in χ'' in ac susceptibility and the temperature variation of the EMR spectra are used to determine the following parameters of the Vogel–Fulcher relaxation for the 3 nm (9 nm) samples respectively: the attempt frequency $f_o = 8 \times 10^{10}$ Hz (2×10^{12} Hz); inter-particle interaction temperature $T_o = 3$ K (33 K) and anisotropy $K_a = 1.96 \times 10^6$ ergs cm^{-3} (4.3×10^5 ergs cm^{-3}). The use of the above parameters for the calculations of the optimum size for magnetic hyperthermia is analysed and discussed.

1. Introduction

The pioneering work of Sun *et al* [1, 2] on the synthesis of FePt nanoparticles (NPs) and the associated discovery of their hard magnetism for potential applications in ultra high-density memory devices has led to many follow-up studies on the Fe_xPt_{100-x} system [2–5]. It is now known that the structure and magnetic properties of Fe_xPt_{100-x} NP depend on x as well as on the annealing temperature T_s. The as-prepared samples are usually in the face-centred-cubic (fcc) phase but annealing the sample above 500 °C leads to the fct ($L1_o$) phase transformation for compositions from $x = 40$ to 70 [4]. Whereas the low-temperature fcc phase has a negligible anisotropy, the fct/$L1_o$ phase is a highly anisotropic ferromagnet. The original paper by Sun *et al* [1] showed a maximum $H_c \approx 4$ kOe for an $Fe_{50}Pt_{50}$ sample annealed at $T_s = 580$ °C. The sample annealed at 580 °C had the crystallite size $D \approx 4$ nm with higher T_s usually leading to larger D and larger blocking temperature T_B. For the $Fe_{55}Pt_{45}$ sample annealed at $T_s = 1000$ °C, $T_B = 530$ K and $H_c = 11$ kOe have been reported [5]. Even $H_c \approx 30$ kOe has been reported in a specially prepared sample of the fct phase [6].

Recently, the low-temperature fcc phase of FePt has also received attention in connection with its possible use as a room temperature superparamagnet (SP) for biomedical applications [7–15]. Since the sizes of the magnetic nanoparticles (MNPs) are quite compatible with cells, proteins and genes and they

[5] Author to whom any correspondence should be addressed.

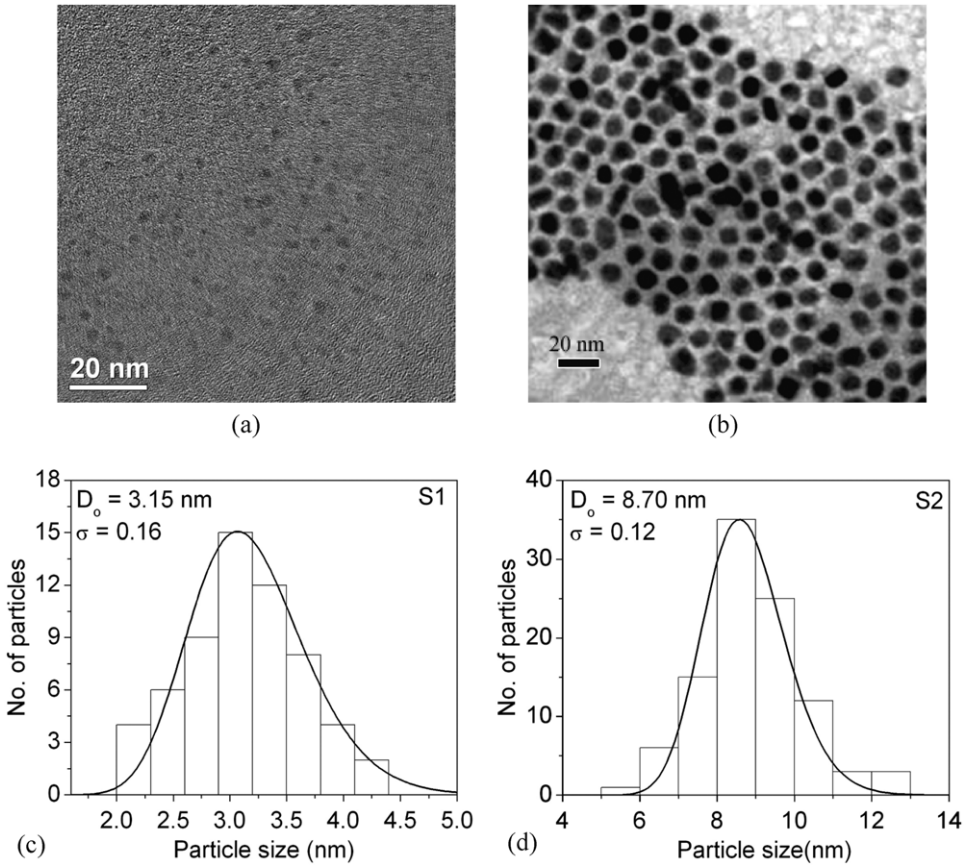

Figure 1. Transmission electron micrographs (TEM) of samples S1 (*a*) and S2 (*b*) with bar lengths = 20 nm. The corresponding histograms of the size distribution are shown in (*c*) and (*d*), respectively, for S1 and S2 with the solid curve showing fits to log-normal distributions.

can be easily manipulated with external magnetic fields, biomedical applications under active consideration include targeted drug delivery, MRI contrast agents, tumour therapy by magnetic hyperthermia and biosensors [7–15]. In [13], a comparative theoretical assessment of magnetic hyperthermia produced by MNPs of magnetite, maghemite, FeCo, $L1_o$ FePt and fcc FePt was presented and it was concluded that among these NPs, fcc FePt NPs have a 'superior ability in magnetic hyperthermia'.

A crucial factor in magnetic hyperthermia is the power P absorbed (dissipated) by NPs of volume V via an orientational relaxation of the magnetic moment in an ac magnetic field of amplitude H_1 and angular frequency $\omega = 2\pi f$ which is given by [11–13]

$$P = \frac{M_s^2 H_1^2 V}{2kT\tau} \frac{\omega^2\tau^2}{1+\omega^2\tau^2}. \quad (1)$$

In equation (1), the dependence of P, and hence the heating produced, on the saturation magnetization M_s and H_1 is straightforward. However, its dependence on the remaining factors of equation (1) is a bit more complicated through the Neel relaxation time $\tau = \tau_o \exp(K_a V/kT)$ of the magnetic moment against the energy barrier $K_a V$, where K_a is the anisotropy constant, $f_o = 1/\tau_o$ is the attempt frequency and k is the Boltzmann constant. In the theoretical analysis of [13] for all the five NPs listed above, $f_o = 10^9$ Hz, $H_1 = 500$ Oe, $f = 300$ kHz and essentially bulk values of M_s independent of volume of V (or size D) of the NPs were used. However, several studies have shown that both K_a and M_s are often size-dependent and f_o is often above 10^9 Hz [16–20]. Also the choice of frequency f for maximum P is dictated by the equality $\omega\tau = 2\pi f\tau = 1$ where the out-of-phase component χ'' of the ac susceptibility and hence P are maximum leading to a maximum power dissipated (equation (1)). Using the parameters listed above and $K_a = 2.06 \times 10^6$ ergs cm^{-3} suitable for 4 nm fcc FePt NPs, the theoretical estimate of [13] determined 9 nm to be the optimum size of fcc FePt NPs for magnetic hyperthermia applications.

From the above considerations, it is evident that magnitudes of M_s, K_a and f_o for different particle sizes should be known for a system for proper choice of the ac frequency f and particle volume V, the latter being important for possible toxicity considerations. In addition, the Neel relaxation is strictly valid only in the absence of inter-particle interactions (IPIs), usually dominated by dipole–dipole interactions. Motivated by these considerations, we report here the first detailed study of the relevant magnetic and relaxation parameters of fcc FePt NPs of nominal sizes $D \simeq 3$ nm (sample S1) and 9 nm (sample S2) by employing the temperature dependence of the ac susceptibilities χ' and χ'' at several frequencies between 0.1 and 1000 Hz, electron magnetic resonance (EMR) spectroscopy at 9.28 GHz and magnetization M versus H and M versus T measurements. These results detailed in the following pages show that the magnitudes of M_s, K_a and f_o are significantly different

for S1 and S2 and some size-dependent IPIs are present in both samples even though the samples are coated with surfactants. These results are applied to the problem of magnetic hyperthermia. Details of these results and their discussion are presented below.

2. Sample preparation

Various procedures used for the synthesis of the Fe_xPt_{100-x} samples have been described in the literature [1–6, 21, 22]. As in many other studies, we used Pt-acetylacetonate (ACROS, 97%) and Fe-pentacarbonyl (Aldrich, 99.99%) as sources for Pt and Fe, respectively, without further purification. Other reagents used were 1,2-hexadecanediol (Aldrich, 90%), dioctylether (ACROS, 90%), benzyl ether (ACROS), oleyl amine (Aldirch, 70%) and oleic acid (Aldrich 90%).

For preparing sample S1 of nominal 3 nm size with $x = 48$, Pt-acetylacetonate (2.4×10^{-4} mole), 1,2-hexadecandiol (7.5×10^{-4} mole) and dioctyl ether (10 ml) were mixed and heated to 100 °C in nitrogen for 10 min. Fe-pentacarbonyl (4.8×10^{-4} mole), oleyl amine (2.5×10^{-4} mole) and oleic acid (2.5×10^{-4} mole) were injected. The reaction mixture was heated to reflux at 297 °C. After 30 min, the heating source was removed and the product was cooled to room temperature. The product was precipitated by adding ethanol and separated by centrifugation. The black product was stored in hexane or toluene.

The key to preparing the larger 9 nm FePt NPs is to increase the surfactant to Pt precursor ratio to at least 8 : 1 and reduce the heating rate to the interim temperature (225 °C) to about 5 °C min^{-1} [21]. In our synthesis of the 9 nm nominal size NPs (labelled here as sample S2) with $x = 48$, Pt-acetylacetonate (2.4×10^{-4} mole) and benzyl ether were mixed and heated to 100 °C in nitrogen. Iron pentacarbonyl (4.8×10^{-4} mole), oleyl amine (1×10^{-3} mole) and oleic acid (1×10^{-3} mole) were added. The reaction mixture was heated to 225 °C at a heating rate of 5 °C min^{-1}. After 1 h, the reaction temperature was raised to 295–300 °C and maintained there for 2 h. The heating mantle was then removed and the product was cooled to room temperature. The product was precipitated by adding ethanol and separated by centrifugation. The black product was stored in hexane or toluene.

3. Experimental results

3.1. Structural characterization

Transmission electron microscopy (TEM) images of the as-synthesized NPs are shown in figure 1(*a*) for the nominal 3 nm NPs and in figure 1(*b*) for the nominal 9 nm NPs. The corresponding histograms of the particle size distributions and their fits to log-normal distribution are shown in figures 1(*c*) and (*d*) with the average sizes of 3.15 nm and 8.70 nm, respectively. The room temperature x-ray diffractograms of the two samples using Cu K_α radiation ($\lambda = 1.541\,85$ Å) show the (1 1 1) and (2 0 0) peaks of the fcc structure with the lattice constant $a = 3.84$ (0.02) Å, with no hint of additional (0 0 1) and (1 1 0) lines characteristic of the fct phase (figure 2). The

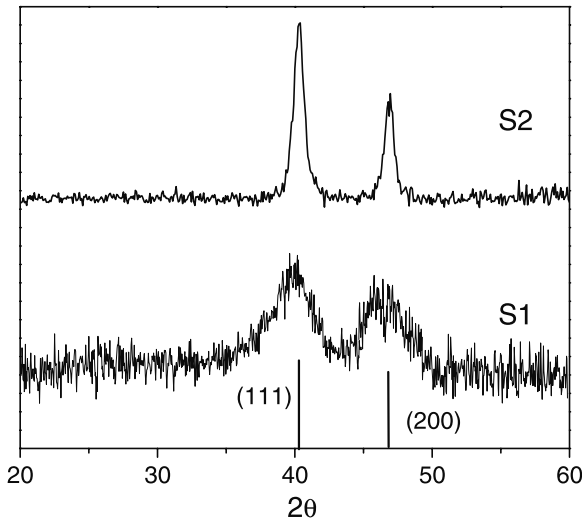

Figure 2. Room temperature x-ray diffraction plots of samples S1 (3 nm) and S2 (9 nm). The miller indices of the two observed Bragg lines for the fcc FePt structure are shown.

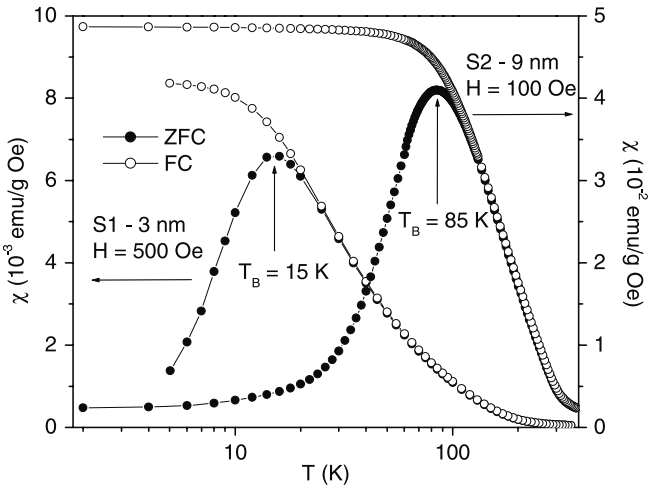

Figure 3. Temperature dependence of the magnetic susceptibility χ under the FC and ZFC modes for samples S1 and S2. The peak position for χ (ZFC) is identified as the average blocking temperature T_B.

sizes determined from the width of the two peaks for S1 and S2 are consistent with the TEM data of figure 1.

3.2. Magnetization

Measurements of magnetization (M) versus temperature and magnetic field (H) were carried out with a commercial superconducting quantum interference device (SQUID) magnetometer. The variation of the magnetic susceptibility $\chi (= M/H)$ with temperature is shown in figure 3. For the zero-field-cooled (ZFC) case, the sample is cooled to 5 K in zero field and a magnetic field is then applied and data are taken with increasing T after stabilizing the temperature at each T. After reaching 350 K, the data are then taken using the same H with decreasing temperature for the field-cooled (FC) case. For sample S1, the data for ZFC peak near $T_B = 15$ K below which the data for FC and ZFC also bifurcate. For sample S2 (9 nm),

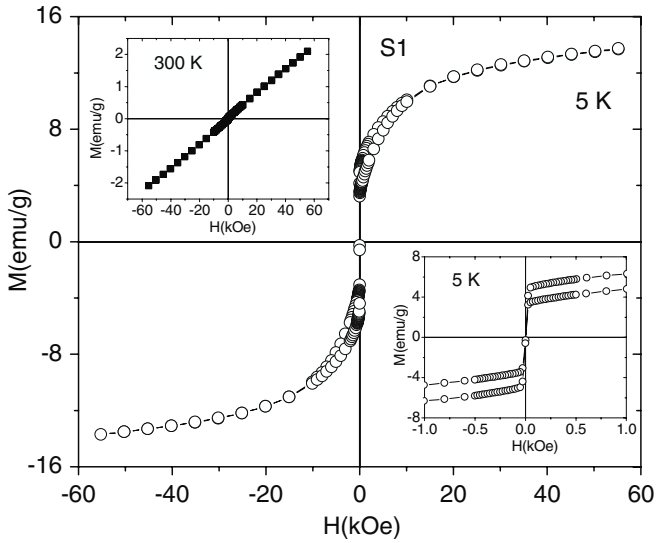

Figure 4. Magnetic hysteresis loops for sample S1 at 5 K with the lower inset showing the details for the low-field region at 5 K. The upper left inset shows M versus H data at 300 K.

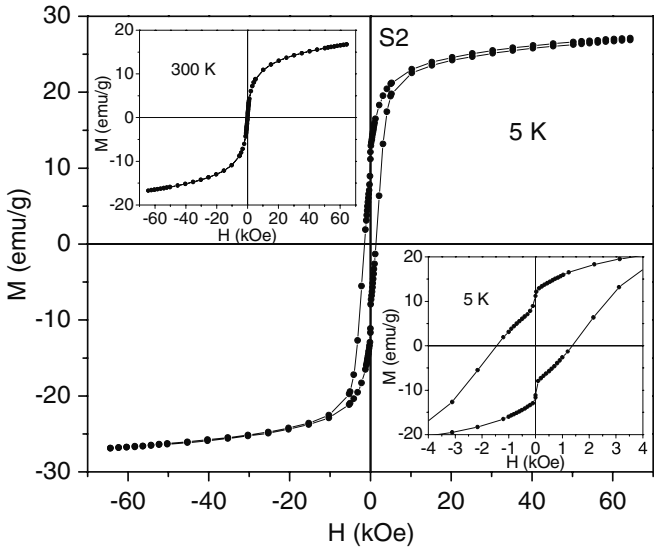

Figure 5. Similar to figure 4 except for sample S2.

$T_B \approx 85$ K is observed. The blocking temperature is associated with the blocking of the thermal switching of the magnetic moments of the majority of the NPs. The fact that the χ (FC) becomes temperature-independent for $T \ll T_B$ suggests that IPI is not negligible even though the particles are coated with surfactants. Additional proof for this is given later from the analysis of the ac susceptibility data.

The magnetic hysteresis loop at 5 K for sample S1 is shown in figure 4 and for sample S2 in figure 5. In the inset of the figures, the hysteresis loops for the low-field region at 5 and at 300 K are shown. It is evident that for S1, coercivity H_c at 5 K ($T < T_B$) is essentially zero within our experimental uncertainties of ± 10 Oe. However, for sample S2 of size 9 nm and $T_B \approx 85$ K, $H_c = 1.5$ kOe at 5 K is measured although $H_c = 0$ Oe at 300 K. The magnetization is not completely saturated even at 65 kOe for both samples. The negligible coercivity for $T \ll T_B$ in the 3 nm fcc FePt is quite unusual for

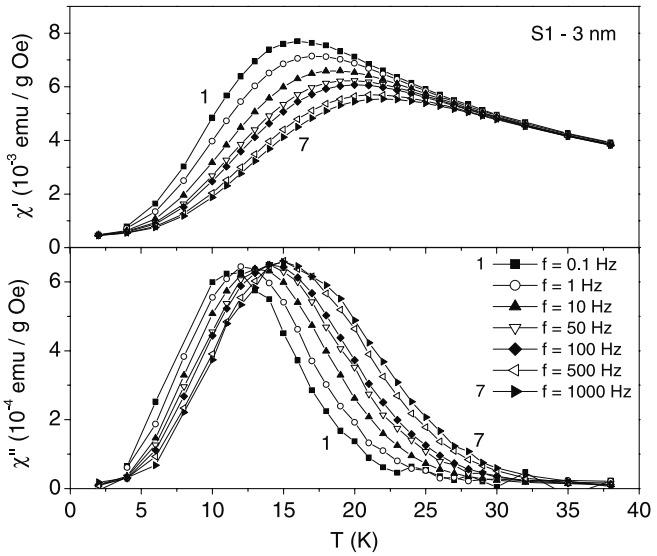

Figure 6. Temperature dependences of the ac susceptibilities χ' and χ'' at the measuring frequencies shown are plotted in (a) and (b), respectively, for sample S1. The lines joining the points are drawn for visual clarity.

MNPs because even for ferromagnetic NPs, such as Ni with $D \approx 3.8$ nm, $H_c \approx 200$ Oe for $T \ll T_B$ is observed [23]. To correct for the mass of the surfactants in the calculations of the M/g of FePt, thermogravimetric analysis (TGA) data were taken by heating the samples in air *in situ* at a rate of $10\,^{\circ}\mathrm{C\,min^{-1}}$ in a TGA balance and measuring the changes in weight with increasing temperatures. As the sample is heated above room temperature, the weight of the sample begins to decrease due to evaporation of the surfactants first slowly, then followed by a rapid decrease near 300 °C, similar to the observations in [24]. Assuming that all the surfactants have evaporated by 400 °C, a correction multiplication factor of 1.33 for the measured magnetization was determined for both the samples. At 300 K, the M versus H plots show superparamagnetism for both samples.

3.3. Frequency dependence of the ac susceptibilities

The ac susceptibilities, χ' and χ'', were also measured with the SQUID magnetometer using $H_{ac} = 6.8$ Oe and $H = 0$ Oe and employing seven measuring frequencies f_m between 0.1 and 1000 Hz. The data of χ' and χ'' versus temperature for S1 are shown in figure 6 and for S2 in figure 7. The positions of the peak in the susceptibilities shift to higher temperatures with increase in the measuring frequency as expected theoretically for MNPs [16, 25]. Also the peak position for χ'' is expected to yield T_B at a particular f_m whereas for χ', the position of maximum in $d\chi'/dT$ is near T_B [16, 25]. The latter is approximately valid in the data shown in figures 6 and 7. The general features of χ' and χ'' versus T curves in figures 6 and 7 are consistent with the simulated curves for weakly interacting NPs via inter-particle dipole interaction [25].

To increase the range of frequencies for measuring the frequency-dependent blocking temperature, we carried out temperature dependence of the EMR spectra of both S1 and S2 at 9.28 GHz using a conventional reflection type spectrometer.

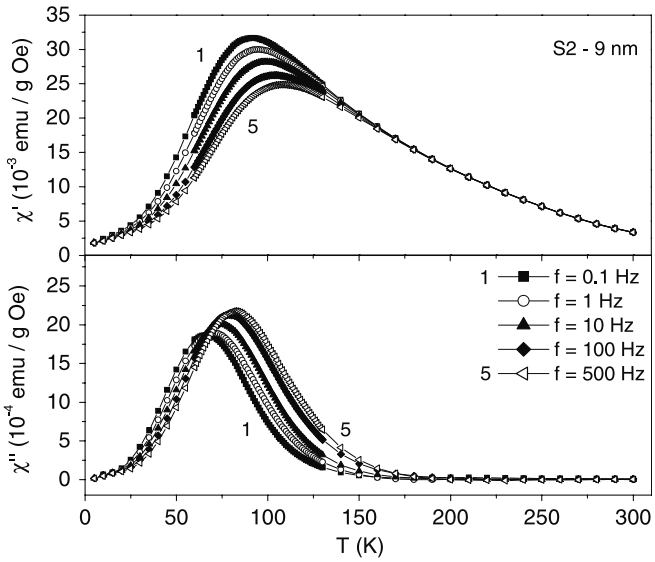

Figure 7. Same as in figure 6 except for sample S2.

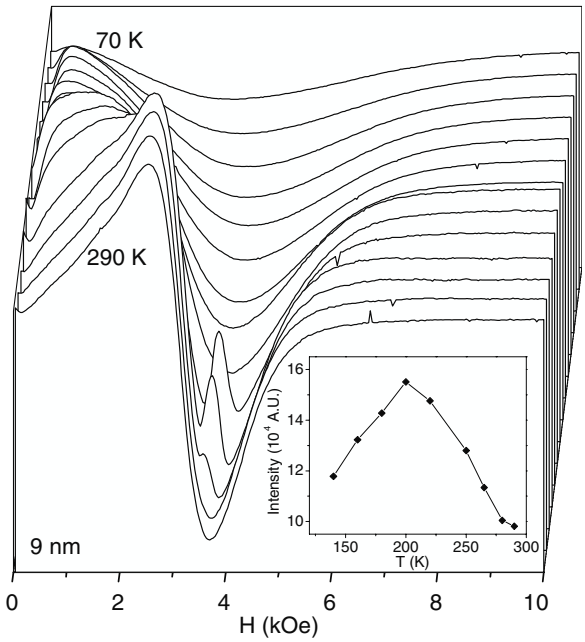

Figure 8. EMR line profiles (first field derivative of absorption) of the 9 nm sample at temperatures $T = 70$, 85, 100, 115, 130, 140, 160, 180, 200, 220, 250, 265, 280 and 290 K. In the inset temperature variation of the intensity of the line is shown (see text for details).

The standard first field derivative of the absorption spectra for the representative sample S2 at different temperatures is shown in figure 8. As the temperature is lowered from 300 K, the spectra at a specific temperature begin to deviate strongly from the symmetric absorption curve along with the appearance of a weaker line which we associate with the onset of the blocking of the moments measured at 9.28 GHz. This onset temperature is 265 K for S2 as evident in figure 8. To determine T_B more accurately, the EMR spectra were integrated to yield the absorption spectra whose full-width at half-maxima ΔH and peak height L were used to determine the variations of the relative intensity $I_o = (\Delta H)L$. The temperature dependence of I_o yields a peak at a specific temperature (see the inset of figure 8) which is associated with $T_B = 200$ K measured at 9.28 GHz, by analogy with T_B measured in the susceptibilities in figures 3, 6 and 7. A similar analysis for S1 yields its $T_B = 110$ K at 9.28 GHz (data not shown). These results combined with T_B determined from the above ac measurements are used later to determine the magnetic relaxation times for S1 and S2.

4. Discussion and interpretation

From the data shown in figures 4 and 5, the saturation magnetization M_s measured at 5 K and 55 kOe equals 14 emu g^{-1} for S1 and 27 emu g^{-1} for S2. Using the calculated density $\rho = 14.77$ g cm^{-3} of fcc FePt with lattice constant $a = 3.84$ Å yields $M_s = 207$ emu cm^{-3} (400 emu cm^{-3}) for S1 (S2). This magnitude of M_s for S1 is in excellent agreement with $M_s = 210$ emu cm^{-3} reported by Wu *et al* [24] on 3.1 nm particles of fcc FePt. Since there are two FePt units per unit cell, this magnitude of M_s gives a magnetic moment $m_s = 0.63\mu_B$/FePt unit for S1. For S2 with 9 nm size, a similar calculation yields $m_s = 1.44\mu_B$/FePt unit. As expected, the magnitude of M_s at 300 K *vis-à-vis* that at 5 K is considerably lower for both samples, being equal to 30 emu cm^{-3} for S1 and 245 emu cm^{-3} for S2. These measurements also show that M_s depends strongly on particle size with M_s decreasing with decreasing particle size. This effect has been reported in other NPs also and it is usually attributed to the role of a magnetically dead surface layer [17–20].

In a recent paper, Jaouen *et al* [26] have reported measurements of spin and orbital magnetic moments in $Fe_{50}Pt_{50}$ NPs using x-ray absorption and magnetic circular dichroism (MCD), at both the Fe and Pt sites. For the disordered fcc phase, they report $m_s = 0.72\mu_B$ at the Fe site and $m_s = 0.30\,\mu_B$ at the Pt site, including several per cent contribution from the orbital moment. After the samples are annealed at 500 °C to convert them to the fct/$L1_o$ phase, nearly 300% increase in the moment with $m_s = 2.20\mu_B$ at the Fe site and $m_s = 0.46\mu_B$ at the Pt site was observed. The above numbers yield a total moment of about $1\mu_B$/FePt in the fcc phase and $2.66\mu_B$/FePt in the ordered $L1_o$ phase. The moment on the Pt site is possibly due to hybridization between 3d orbitals of Fe and 5d orbitals of Pt. So in the fcc phase, not only are the atoms in random sites and disordered, but the magnetic moments are also only partially ordered. Our measured value of $m_s = 0.63\mu_B$/FePt unit for S1 in the fcc phase is in agreement with $m_s = 0.66\mu_B$/FePt measured by SQUID magnetometry as reported by Jaouen *et al* on their 3 nm fcc FePt NPs [26]. In the calculations of Maenosono *et al* for magnetic hyperthermia [13], $M_s = 1140$ emu cm^{-3} was assumed for fcc FePt for the 9 nm optimum size for magnetic hyperthermia. Our data show that $M_s = 400$ emu cm^{-3} (245 emu cm^{-3}) at 5 K (300 K) for the 9 nm fcc FePt NPs.

Although the magnitude of M_s does not affect the optimum size for magnetic hyperthermia, the magnitude of τ in equation (1), which in turn is determined by the anisotropy constant K_a and the attempt frequency f_o, does affect the calculation of the optimum size. These quantities

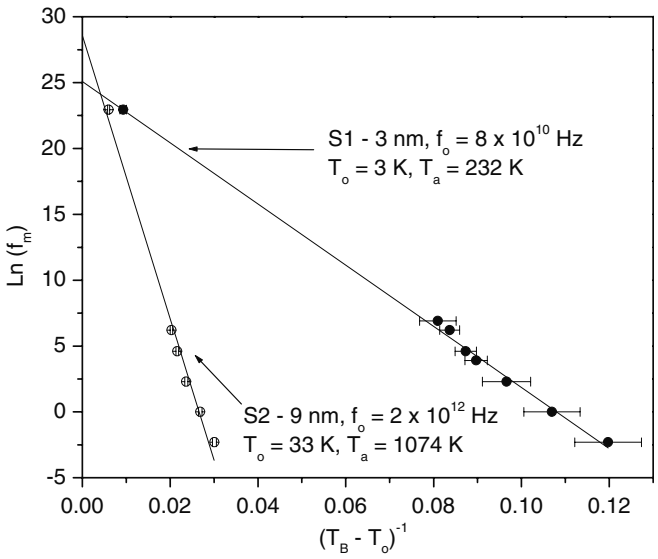

Figure 9. ln f_m is plotted against $1/(T_B - T_o)$ for samples S1 and S2 following equation (2) with intercepts yielding ln f_o and slopes yielding T_a as shown in the figure.

are determined from the analysis of the variation of T_B with measuring frequency f_m using the procedures described in a recent paper [16]. For weakly interacting NPs of volume V, T_B can be written as [16, 18–20, 27]

$$T_B = T_o + T_a/\ln(f_o/f_m). \quad (2)$$

Here $T_a = K_a V/k$ with k being the Boltzmann constant and T_o is a measure of the strength of the IPI. For non-interacting NPs, $T_o = 0$ K and equation (2) reduces to the expression for the Neel–Brown relaxation. Using the procedures developed in our recent paper [16] and data of T_B determined at different f_m in section 3.3, T_o, K_a and f_o are evaluated in the plots of figure 9 based on equation (2). In developing these fits, T_o is varied until the data fall on a straight line in the plot of ln f_m versus $(T_B - T_o)^{-1}$, with the intercept yielding ln f_o and the slope T_a. The magnitudes of these parameters are listed in figure 9 for both S1 and S2. The larger magnitude of T_o for S2 (33 K) than that for S1 (3 K) suggests a stronger IPI in S2, as also confirmed below by another calculation. The evaluated attempt frequency $f_o \approx 8 \times 10^{10}$ Hz for S1 and $f_o \approx 2 \times 10^{12}$ Hz for S2. Both these magnitudes of f_o are certainly larger than $f_o = 10^9$ Hz assumed in the calculations of [13]. The magnitude of $T_a = K_a V/k = 232$ K for S1 yields $K_a = 1.96 \times 10^6$ ergs cm^{-3} assuming spherical particles of diameter $D = 3.15$ nm. A similar calculation for S2 with $T_a = 1074$ K and $D = 8.7$ nm yields $K_a = 4.30 \times 10^5$ ergs cm^{-3}. The increase in K_a with decreasing particle size calculated above has been observed in other systems also and this increase is generally attributed to increasing contribution from surface anisotropy in smaller particles [16, 18–20]. In the calculations of [13], $K_a = 2 \times 10^6$ ergs cm^{-3} was assumed, which is appropriate for about 3 nm fcc FePt NPs. The larger magnitudes of f_o determined above for S2 are most likely due to the presence of larger IPI as manifested in the larger T_o [18, 28–30].

The strength of IPI in a given system can also be estimated by determining the quantity [27]

$$\Phi = \Delta T_B/\left[T_B \Delta \log_{10} f_m\right]. \quad (3)$$

Here ΔT_B is the change in T_B determined from the χ'' versus T data (figures 6 and 7) with measuring frequency f_m. The expected magnitudes of Φ are 0.005–0.05 for spin glasses; $\Phi = 0.13$ for isolated NPs whereas the range $0.05 < \Phi < 0.13$ represents interacting NPs with the strength of coupling decreasing with increasing Φ [27]. For the data for S1 in figure 6, $\Phi = 0.09(1)$ is estimated whereas a similar analysis for S2 from the data in figure 7 yields $\Phi = 0.066(10)$. Thus both samples have non-negligible IPI, the effect being smaller in the smaller particles (S1). This is in agreement with the magnitudes of $T_o = 3$ K (33 K) determined earlier for S1 (S2). Despite the coating by surfactants, the effect of IPI is present in these samples possibly because of the long-range nature of the dipole–dipole interaction. The larger effect in S2 *vis-à-vis* S1 is likely due to its larger M_s as compared with that for S1 as shown earlier.

In magnetic hyperthermia experiments, magnetic particles are usually suspended in body-friendly fluids such as water. In such cases, the relaxation rate is the sum of the Brownian relaxation rate of the particles in the fluid and the Neel relaxation rate of the superparamagnetic particles (such as fcc FePt NPs) determined here [11–13]. In the theoretical analysis of Maenosono *et al* [13], a 10% concentration of the MNPs in water was considered along with size-independent $f_o = 10^9$ Hz. To calculate the optimum volume V and hence diameter D of a NP at a temperature T for magnetic hyperthermia, the equality $2\pi f\tau = 1$ is used where $\tau = \tau_o \exp[T_a/(T - T_o)]$ with $\tau_o = 1/f_o$ and $T_a = K_a V/k$ for the Neel relaxation. This calculation requires the magnitudes of K_a, T_o and τ_o. Assuming the magnitudes of $K_a = 2 \times 10^6$ ergs cm^{-3}, $T_o = 0$ K and $f_o = 10^9$ Hz, as done in [13], yields the optimum $D = 6.2$ nm for fcc FePt at the operating frequency $f = 300$ kHz and $T = 300$ K without including the effect of Brownian relaxation. With Brownian relaxation included, optimum $D = 9$ nm was calculated in [13]. From the analysis in the preceding paragraph, it is evident that these magnitudes of K_a and f_o are not valid for 9 nm NPs of fcc FePt. If we use $K_a = 4.3 \times 10^5$ ergs cm^{-3}, $T_o = 33$ K and $f_o = 2 \times 10^{12}$ Hz determined here for 9 nm size, then the optimum size $D = 13.1$ nm is calculated for $f = 300$ kHz at 300 K considering only the Neel relaxation. For $f = 120$ kHz, which is considered to be a safer operating frequency [31], $D = 13.4$ nm as the optimum size is obtained for the Neel relaxation. Hence unless the Brownian relaxation rate completely dominates the Neel relaxation rate, the optimum size of the NPs for magnetic hyperthermia applications will depend on quantities such as f_o and K_a, which as shown here for the fcc FePt NPs are strongly size dependent. In particular f_o for the FePt NPs is over two orders of magnitude larger than 10^9 Hz assumed in the previous theoretical analysis of this problem [11, 13]. These considerations need to be taken into account in future investigations of magnetic hyperthermia.

5. Concluding remarks

In this work, measurements of the magnetic and relaxation parameters of MNPs of fcc FePt are presented for two samples with nominal sizes of 3 nm and 9 nm. These measurements show that these parameters are strongly dependent on the particle size, in that the anisotropy constant increases with decreasing particle size whereas the opposite is valid for the saturation magnetization M_s, the relaxation frequency f_o, the blocking temperature T_B and the IPI. In particular, the experimentally determined magnitude of f_o is about two orders of magnitude larger than 10^9 Hz assumed in a previous theoretical analysis of magnetic hyperthermia [11, 13]. The numerical values of these parameters are then used for the calculations of the optimum size of fcc FePt for magnetic hyperthermia applications for the Neel relaxation. The need to take into account the size dependence of the magnetic and relaxation parameters of superparamagnetic particles for magnetic hyperthermia applications has been demonstrated.

References

[1] Sun S, Murray C B, Weller D, Folks L and Moser A 2000 *Science* **287** 1989
[2] Sun S A, Thomson T, Baglin J E E, Toney F M, Hamann H F, Murray C B and Terris B D 2003 *J. Phys. Chem.* B **107** 5419
[3] Rellinghaus B, Stappert S, Acet M and Wassermann E F 2003 *J. Magn. Magn. Mater.* **266** 142
[4] Rong C B, Li Y and Liu J P 2007 *J. Appl. Phys.* **101** 09K505
[5] Varanda L C and Jafelicci M Jr 2006 *J. Am. Chem. Soc.* **128** 11062
[6] Li D, Poudyal N, Nandwana V, Zin Z, Elkins K and Liu J P 2006 *J. Appl. Phys.* **99** 08E911
[7] Hergt R, Andra W, d'Ambly C G, Hilger I, Kaiser W A, Richter U and Schmidt H G 1998 *IEEE Trans. Magn.* **34** 3745
[8] Pankhurst Q A, Thanh N K T, Jones S K and Dobson J 2009 *J. Phys. D: Appl. Phys.* **42** 224001
Pankhurst Q A *et al* 2003 *J. Phys. D: Appl. Phys.* **36** R167
[9] Berry C C 2009 *J. Phys. D: Appl. Phys.* **42** 224003
Roca A G *et al* 2009 *J. Phys. D: Appl. Phys.* **42** 224002
[10] Neuberger T, Schopf B, Hofmann H, Hofman M and Rechenberg B V 2005 *J. Magn. Magn. Mater.* **293** 483
[11] Rosensweig E 2002 *J. Magn. Magn. Mater.* **252** 370
[12] Hergt R and Dutz S 2007 *J. Magn. Magn. Mater.* **311** 187
[13] Maenosono S and Saita S 2006 *IEEE Trans. Magn.* **42** 1638
Maenosono S, Suzuki T and Saita S 2008 *J. Magn. Magn. Mater.* **320** L79
[14] Nikitin P, Vetoshko P M and Ksenevich T I 2007 *J. Magn. Magn. Mater.* **311** 445
[15] Chung S H, Hoffmann A, Bader S D, Liu C, Kay B, Makowski L and Chen L 2004 *Appl. Phys. Lett.* **85** 2971
[16] Singh V, Seehra M S and Bonevich J 2009 *J. Appl. Phys.* **105** 07B518
[17] Dutta P, Pal S, Seehra M S, Shah N and Huffman G P 2009 *J. Appl. Phys.* **105** 07B501
[18] Yanes R, Fesenko C, KachKachi H, Garanin D A, Evans R and Chantrell R W 2007 *Phys. Rev.* B **76** 064416
[19] Bodkar F, Morup S and Linderoth S 1994 *Phys. Rev. Lett.* **72** 282
[20] Gilmore K, Idzerda U, Klem M T, Allen M, Douglas T and Young M 2005 *J. Appl. Phys.* **97** 10B301
[21] Sun S 2006 *Adv. Mater.* **18** 393
[22] Wellons M S, Morris III W H, Gai Z, Shen J, Bentley J, Wittig J E and Lukehart C M 2007 *Chem. Mater.* **19** 2483
[23] Singh V, Seehra M S and Bonevich J 2008 *J. Appl. Phys.* **103** 07D524
[24] Wu X W, Liu C, Li L, Jones P, Chantrell R W and Weller D 2004 *J. Appl. Phys.* **95** 6810
[25] Anderson J O, Djurberg C, Jonsson T, Svedlindh P and Nordblad P 1997 *Phys. Rev.* B **56** 13983
[26] Jaouen N, Babonneau D, Tonnerre J M, Carbone D, Wilhelm F, Rogalev A, Johal T K and Laan G V 2007 *Phys. Rev.* B **76** 104421
[27] Dormann J L, Bessais L and Fiorani D 1988 *J. Phys. C: Solid State Phys.* **21** 2015
[28] Berger L, Labaye Y, Tamine M and Coey J M D 2008 *Phys. Rev.* B **77** 104431
[29] Shim H, Dutta P, Seehra M S and Bonevich J 2008 *Solid State Commun.* **145** 192
[30] Shim H, Manivannan A, Seehra M S, Reddy K M and Punnoose A 2006 *J. Appl. Phys.* **99** 08Q503
[31] Okawa K, Sekine M, Maeda M, Tada M, Abe M, Matsushita N, Nishio K and Handa H 2006 *J. Appl. Phys.* **99** 08H102